ELSEVIER

Materials Science and Engineering A 438–440 (2006) 536–539

MATERIALS SCIENCE & ENGINEERING A

www.elsevier.com/locate/msea

Electrical resistivity of Ti–Ni binary and Ti–Ni–X (X = Fe, Cu) ternary shape memory alloys

S.K. Wu *, H.C. Lin, T.Y. Lin

Department of Materials Science and Engineering, National Taiwan University, Taipei 106, Taiwan, ROC

Received 25 April 2005; received in revised form 21 November 2005; accepted 9 December 2005

Abstract

The electrical resistivities of Ti–Ni binary and Ti–Ni–X (X = Fe, Cu) ternary shape memory alloys (SMAs) are investigated. Experimental results reveal that the Ti–Ni and Ti–Ni–X SMAs exhibit different electrical resistivity (ρ) characteristics due to their different martensitic transformation behaviors. The increase of ρ during the B2 → R transformation of Ti–Ni SMAs is about 10–16 μΩ cm, which is a change of about 12–20%. For a two-stage transformation of B2 ↔ R ↔ B19′, there is a sharp increase of ρ during B2 → R transformation, and then a rapid decrease of ρ during R → B19′ transformation. However, for the Ti-40 at.%,Ni-10 at.%,Cu alloy, which exhibits a B2 ↔ B19 ↔ B19′ two-stage transformation, there is a small variation of ρ during B2 → B19 transformation, but a significant variation of ρ during B19 → B19′ transformation. These phenomena may be ascribed to their different structures, deformation defects, accommodated twin variants and crystal distortions.

Keywords: Ti–Ni shape memory alloys; Electrical resistivity; Martensitic transformation

1. Introduction

Among many shape memory alloys (SMAs), TiNi-based alloys are most popular because they have superior properties in shape memory effect (SME) and pseudoelasticity (PE) [1–3]. They have a fast and accurate shape memory response to temperature change and are widely used in both medical and industrial applications, such as the orthodontic products, medical implants and stents, controllers and sensors. In addition to the applications of SME and PE, Ti–Ni alloys can exhibit excellent performance of mechanical damping, thermal expansion and electrical resistivity (ER) variation due to their thermoelastic martensitic transformations. These unique properties are expected to have many potential applications in the near future through further studies. It is well known that the transformation behaviors of Ti–Ni SMAs, involving the variation of transformation temperatures and the occurrence of multi-stage transformation sequences, can be affected by various thermo-mechanical treatments [4–7] and the addition of the third or fourth elements [8–11]. For the investigations of Ti–Ni SMAs, ER measurement has been a well-known technique for understanding their transformation behaviors [12–15]. There are distinguished variations of electrical resistivity for different phases of Ti–Ni SMAs, including the B2 parent, B19′ martensite, and intermediate R and B19 phases. Based on the change of the electrical resistivity versus temperature, it is quite effective to identify the transformation behaviors of these phases. Due to the difficulty in the temperature control and the difference in the specimen dimension, the ER (ρ) is not easily measured in the early investigations by using the four-probe DC current technique. However, these technical problems have been overcome in this study by using a precise heating/cooling controller, an accurate measuring equipment of electrical resistivity and the meticulous preparation of testing specimens. Therefore, very precise ρ values for various phases of Ti–Ni SMAs can be measured. The affecting factors on the ρ values and the martensitic transformations of various TiNi-based SMAs are also discussed in this paper.

2. Experimental procedure

The conventional tungsten arc-melting technique was employed to prepare the Ti–Ni binary and Ti–Ni–X (X = Fe, Cu) ternary alloys. Titanium (purity, 99.7%), nickel (purity, 99.98%), and iron (purity, 99.95%) or copper (purity, 99.9%), totaling about 120 g, were melted and remelted at least six times in an

* Corresponding author. Tel.: +886 2 23637846; fax: +886 2 23634562.
E-mail address: skw@ntu.edu.tw (S.K. Wu).

0921-5093/$ – see front matter © 2006 Elsevier B.V. All rights reserved.
doi:10.1016/j.msea.2005.12.059

argon atmosphere. The as-melted buttons were hot-rolled into plates of 2 mm thickness at 800 °C. Specimens with a dimension of 2 mm × 2 mm × 40 mm were carefully cut from these plates with a low-speed diamond saw. For Ti–Ni–X (X = Fe, Cu) ternary alloys, some hot-rolled specimens were solution-treated at 800 °C for 2 h and then quenched in water. For Ti-51 at.%Ni alloy, the hot-rolled specimens were aged at 400 °C for 24 h and then quenched in water. The precise four-probe DC current technique was used to measure the ER (ρ) of Ti–Ni binary and Ti–Ni–X (X = Fe, Cu) ternary alloys. The ER (ρ) is measured at temperatures ranging from −150 to +150 °C under a controlled cooling/heating rate of 10 K/min. A Keithley 2000 Multimeter is used to measure the voltage between the two inner probes while a constant current is passed through the two outer probes using a GP0250-3R DC power supply. The precision of the ER measurement is ±0.1 μΩ cm. The recording of data is completely automatic; calculation and plotting points for the ρ versus temperature are carried out by a digit computer. Thus the results with a rather good resolution can be obtained. The DSC measurement was conducted with a DuPont 2000 thermal analyzer equipped with a quantitative scanning system 910 DSC cell. The cooling/heating rate was precisely controlled at 10 K/min.

3. Results and discussion

Fig. 1 shows the curves of ρ versus temperature for the as hot-rolled Ti-50 at.%Ni alloy. The curves exhibit the typical forward and reverse martensitic transformations of Ti–Ni SMAs. The notation for determining the transformation temperatures on the ER curves follows the example established by Hwang et al. [16]. In Fig. 1, we can find that the ρ values of both B2 phase and B19′ martensite decrease with decreasing temperature. This behavior is similar to that for the general pure metals [17]. Meanwhile, there is a significant increment of ρ value prior to the Ms temperature in Fig. 1. This feature is considered to be related to the formation of R-phase prior to the martensitic transformation. As compared the ER curves in Fig. 1 with those of the solution-treated Ti-50 at.%Ni specimens in a reported paper [18] and those of our unpublished data, the ER curves shown in Fig. 1 are quite similar to those of the solution-treated specimens. It indicates that the formation of R-phase prior to the martensitic transformation may occur in both the as hot-rolled and the solution-treated Ti-50 at.%Ni specimens. This phenomenon is reasonable because the internal stress introduced by hot-rolling

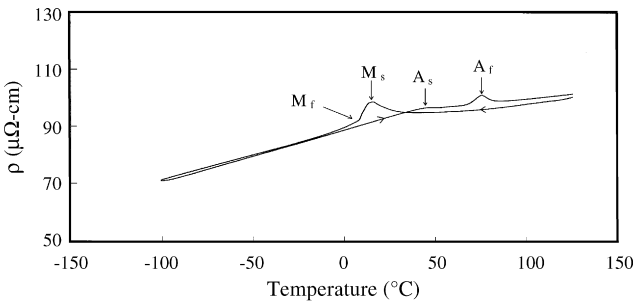

Fig. 1. The curve of ρ vs. temperature for the as hot-rolled Ti-50 at.%Ni alloy.

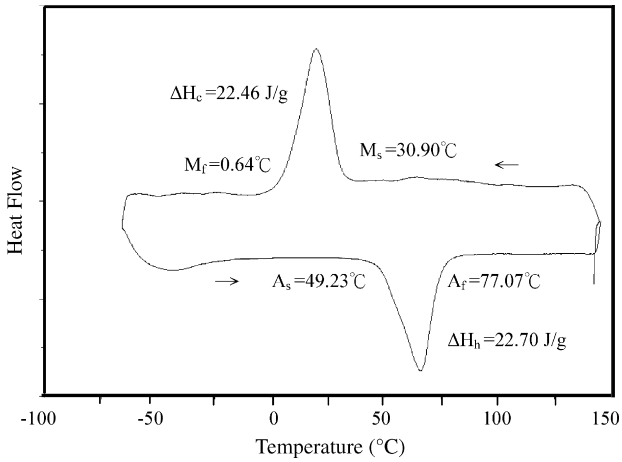

Fig. 2. The DSC curve for the as hot-rolled Ti-50 at.%Ni alloy.

and rapid-quenching after solution treatment will assist the formation of R-phase. The increment of ρ value associated with the R-phase transformation will be discussed later.

Fig. 2 shows the DSC curves for the as hot-rolled Ti-50 at.%Ni alloy. As carefully examining the transformation temperatures in Figs. 1 and 2, one can find that the Ms temperature in the DSC curve is a little higher than that in the ER curve. This phenomenon can be explained as follows. Because the R-phase and martensitic transformations can not be completely separated in the DSC curve for the as hot-rolled Ti-50 at.%Ni specimen in this study, there only appears an exothermic peak in the cooling curve. This exothermic peak, being contributed from both R-phase and martensitic transformations, will exhibit a little higher Ms temperature than that in the ER curve, where the Ms temperature only indicates the start of R → B19′ transformation.

It is well known that the thermal aging of Ni-rich alloys at 300–500 °C will cause the formation of Ti_3Ni_4 precipitates accompanied by the appearance of R-phase transformation [5,19]. Fig. 3 shows the curve of ρ versus temperature for the Ti-51 at.%Ni alloy aged at 400 °C for 24 h. It shows that ρ increases by 12 μΩ cm during the B2 → R transformation and decreases by 25 μΩ cm during the R → B19′ transformation.

Fig. 4 shows the curve of ρ versus temperature for the solution treated Ti-48.5 at.%Ni-1.5 at.%Fe alloy. The curve of ρ versus temperature is similar to that for 400 °C, 24 h aged Ti-

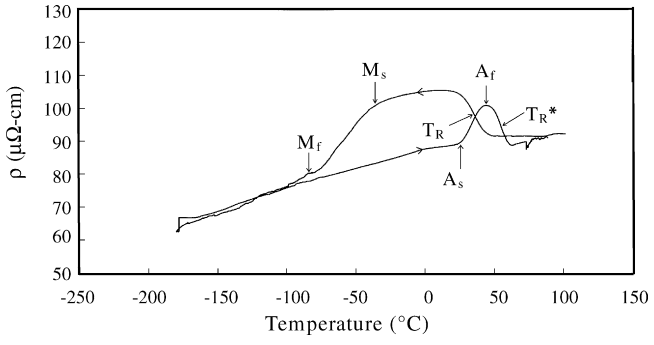

Fig. 3. The curve of ρ vs. temperature for the Ti-51 at.%Ni alloy aged at 400 °C for 24 h.

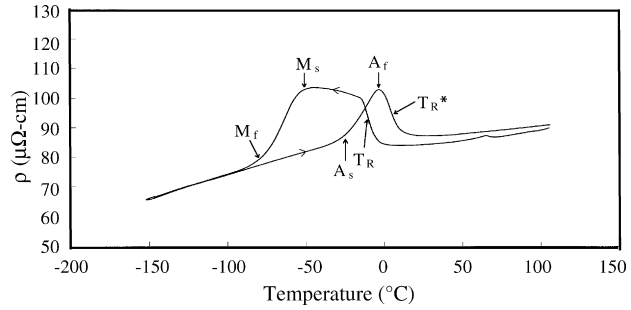

Fig. 4. The curve of ρ vs. temperature for the solution treated Ti-48.5 at.%Ni-1.5 at.%Fe alloy.

51 at.%Ni alloy, except that ρ has a higher increase during the B2 → R transformation, say, 16 μΩ cm. Fig. 5(a) shows the curve of ρ versus temperature for the as hot-rolled Ti-48.5 at.%Ni-1.5 at.%Fe specimen. As compared with Fig. 4, the transformation temperatures of B2 → R and R → B19′ are depressed to lower ones, but the transformation temperatures of R → B2 and B19′ → R are raised to higher ones. It indicates that the hot rolling will inhibit both forward and reverse transformations during the cooling and heating cycles, respectively. This feature may be ascribed to the deformation defects introduced by the hot rolling, and will increase the thermal hysteresis during the forward and reverse transformations. After annealing of 650 °C for 1 h and then furnace cooling, the deformation defects will be died out, and hence the curve of ρ versus temperature, as shown in Fig. 5(b), will recover to a normal one, which is similar to that of Fig. 4.

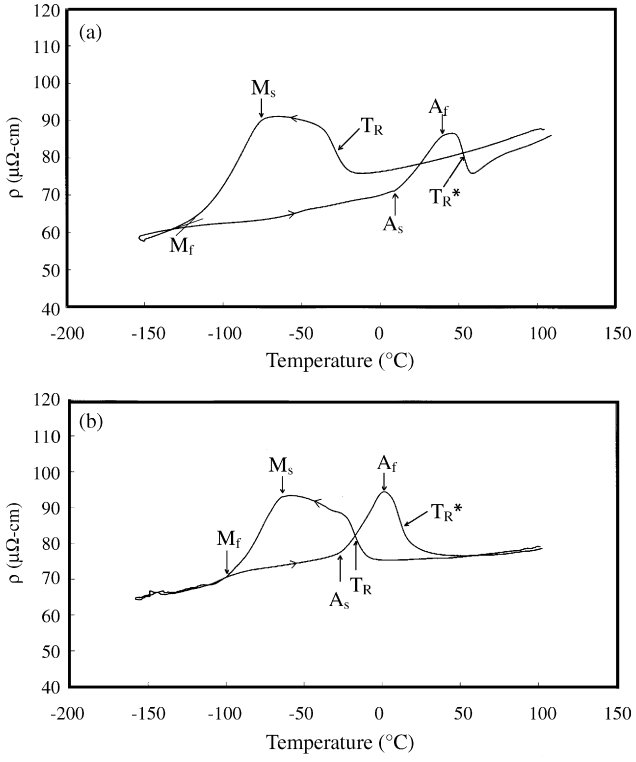

Fig. 5. The curve of ρ vs. temperature for (a) the as hot-rolled and (b) the hot-rolled and subsequently annealed (650 °C, 1 h) Ti-48.5 at.%Ni-1.5 at.%Fe specimen.

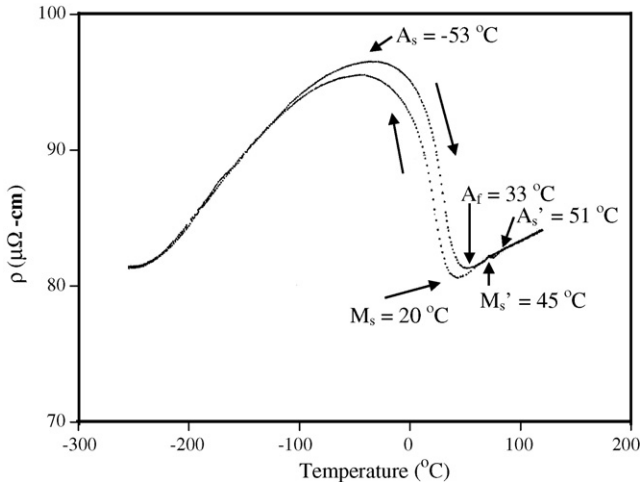

Fig. 6. The curve of ρ vs. temperature for the Ti-40 at.%Ni-10 at.%Cu alloy [20].

For the two-stage transformation of B2 ↔ R ↔ B19′, as shown in Figs. 3–5, there is a sharp increase of ρ during B2 → R transformation, and then a dramatic decrease of ρ during R → B19′ transformation. However for the Ti-40 at.%Ni-10 at.%Cu alloy, which exhibits a B2 ↔ B19 ↔ B19′ two-stage transformation, there is a quite different variation of ρ. As shown in Fig. 6, the B2 → B19 transformation has a small variation of ρ, but there is a significant variation of ρ during B19 → B19′ transformation [20]. This phenomenon can be explained as below. There are many planar twin variants in the B19′ martensite, but not in the B19 martensite [21]. Therefore, the variation of ρ during B2 → B19 transformation is small because no planar twin variants are introduced. But the variation of ρ at B19 → B19′ transformation is significant because a lot of planar twin variants and monoclinic distortion are introduced. During the B2 → R transformation, the accommodation of four R-phase variants with ⟨1 1 1⟩ elongated directions will introduce lots of twin defects and rhombohedral distortion [22,23]. This rises up the ρ of R phase and then reduces to a lower ρ after R → B19′ transformation because the ρ value of B19′ at M_f temperature is almost the same as that of B2 parent phase, as indicated in Fig. 1. Based on the above discussion, the crystal structures, deformation defects, accommodated twin variants and crystal distortions of Ti–Ni SMAs will all have contributions to their specific electrical resistivity.

4. Conclusions

The crystal structures, deformation defects, accommodated twin variants and crystal distortions will all have contributions to the electrical resistivity (ρ) of Ti–Ni SMAs. The increase of ρ value during the B2 → R transformation is about 10–16 μΩ cm, which is about 12–20% change. For a two-stage transformation of B2 ↔ R ↔ B19′, there is a sharp increase of ρ during B2 → R transformation, and then a dramatic decrease of ρ during R → B19′ transformation. However, for the Ti-40 at.%Ni-10 at.%Cu alloy, which exhibits a B2 ↔ B19 ↔ B19′ two-stage transformation, there is a small variation of ρ during

B2 → B19 transformation, but a significant increase of ρ during B19 → B19′ transformation.

Acknowledgement

The authors gratefully acknowledge the financial support of this research by the National Science Council (NSC), Republic of China, under Grants NSC93-2216-E002-003 and NSC88-2216-E002-012.

References

[1] C.M. Jackson, H.J. Wagner, R.J. Wasilewski, NASA Report SP-5110, Washington, DC, 1972. pp. 23–55.
[2] S. Miyazaki, T. Imai, Y. Igo, K. Otsuka, Metall. Trans. A17 (1986) 115.
[3] S.K. Wu, H.C. Lin, Mater. Chem. Phys. 64 (2000) 81.
[4] S. Miyazaki, Y. Igo, K. Otsuka, Acta Metall. 34 (1986) 2045.
[5] S.K. Wu, H.C. Lin, T.S. Chou, Acta Metall. 38 (1990) 95.
[6] H.C. Lin, S.K. Wu, T.S. Chou, H.P. Kao, Acta Metall. Mater. 39 (1991) 2069.
[7] H.C. Lin, S.K. Wu, Acta Metall. Mater. 42 (1994) 1623.
[8] Y.C. Lo, S.K. Wu, C.M. Wayman, Scripta Metall. Mater. 24 (1990) 1571.
[9] M. Piao, S. Miyazaki, K. Otsuka, Mater. Trans. J. Inst. Met. 33 (1992) 346.
[10] H.C. Lin, K.M. Lin, S.K. Chang, C.S. Lin, J. Alloys Compd. 284 (1999) 213.
[11] H.C. Lin, C.H. Yang, K.M. Lin, G.K. Hsu, J. Alloys Compd. 386 (2005) 157.
[12] M.G. Faulkner, J.J. Amalraj, A. Bhattacharyya, Smart Mater. Struct. 9 (2000) 632.
[13] T.H. Nam, G.S. Ha, H.W. Lee, S.G. Hur, Mater. Sci. Technol. 16 (9) (2000) 1017.
[14] M. Pozi, G. Airoldi, Mater. Sci. Eng. A273–A275 (1999) 300.
[15] J. Uchil, K.K. Mahesh, K. Ganesh Kumara, Physica B324 (2002) 419.
[16] C.M. Hwang, M. Meichle, M.B. Salamon, C.M. Wayman, Philos. Mag. A47 (1983) 9.
[17] William F. Smith, Foundations of Materials Science and Engineering, 3rd ed., McGraw-Hill, New York, USA, 2003.
[18] S. Miyazaki, S. Kimura, K. Otsuka, Philos. Mag. A57 (1988) 467.
[19] S.K. Wu, H.C. Lin, Scripta Metall. Mater. 25 (1991) 1295.
[20] Y.C. Lo, S.K. Wu, H.E. Horng, Acta Metall. Mater. 41 (1993) 747.
[21] T. Saburi, Y. Watanabe, S. Nenno, ISIJ Int. 29 (1989) 405.
[22] H.C. Ling, R. Kaplow, Metall. Trans. A11 (1980) 77.
[23] M.B. Salamon, M. Meichle, C.M. Wayman, Phys. Rev. B31 (1985) 7306.